^{3}He(γ, pd) cross sections with tagged photons below the Δ resonance

N. R. Kolb, E. B. Cairns, E. D. Hackett, E. Korkmaz, T. Nakano, A. K. Opper, M. A. Quraan, N. L. Rodning, and F. M. Rozon
Centre for Subatomic Research, University of Alberta, Edmonton, Alberta, Canada T6G 2N5

J. Asai, G. Feldman, E. Hallin, G. V. O'Rielly, R. E. Pywell, and D. M. Skopik
Saskatchewan Accelerator Laboratory, Saskatoon, Saskatchewan, Canada S7N 0W0
(Received 20 May 1993; revised manuscript received 13 January 1994)

The reaction cross section for ^{3}He(γ, pd) has been measured using the Saskatchewan-Alberta Large Acceptance Detector (SALAD) with tagged photons in the energy range from 166 to 213 MeV. The energy and angle of the proton and the deuteron were measured with SALAD while the tagger determined the photon energy. Differential cross sections have been determined for $40° < \theta_p^* < 150°$. The results are in agreement with the Bonn and Saclay photodisintegration measurements. The most recent photodisintegration measurement performed at Bates is higher by a factor of 1.3, which is just within the combined errors of the experiments. The proton capture results differ by a factor of 1.7 from the present experiment. Comparisons are made with microscopic calculations of the cross sections.

PACS number(s): 25.20.Lj, 25.10.+s, 21.45.+v

I. INTRODUCTION

The photodisintegration of ^{3}He is an excellent testing ground for our theoretical knowledge of the fundamental interaction among nucleons in a nucleus [1, 2]. The electromagnetic interaction is well understood and the ground-state wave function can be calculated "exactly" through the use of Faddeev techniques. Requiring that theory reproduce the photodisintegration of the deuteron, as well as the two-body photodisintegration of ^{3}He, places stringent constraints on the calculations. The three-body breakup channel of ^{3}He may be examined for deviations from the calculations which would be indicative of ingredients missing from the theory. These may consist of a deficiency in describing the final-state continuum wave function, or more interestingly, evidence for three-nucleon forces. A measurement of the ^{3}He(γ, pd) reaction will be discussed in this paper. A later paper will report the three-body cross sections obtained simultaneously with the two-body data.

Several measurements of cross sections for the two-body photodisintegration of ^{3}He and the inverse reaction (radiative capture) have been done in the past, as tests of time-reversal invariance [3–12]. For incident proton energies below 200 MeV (corresponding to photon energies below 140 MeV) the Illinois result [3] is in good agreement with the capture measurements of the Orsay group [4] and, more recently, with those at the Indiana University Cyclotron Facility (IUCF) [5]. For higher energies, the agreement among the capture measurements is good, although deviations of up to 35% between the TRIUMF [6] and SATURNE [7] data are seen for incident proton energies above 400 MeV ($E_\gamma > 270$ MeV). The photodisintegration experiments have shown deviations, among themselves and with the capture results, by as much as a factor of 3. The most recent photodisintegration measurement at Bates [8] finds cross sections in agreement within errors with the capture measurements at SATURNE and IUCF. All of these are in agreement with the Illinois results where they overlap, but are significantly higher than the Saclay [9] and Bonn [10] measurements. The Frascati [11] and Caltech [12] results are higher by factors from 1.8 to 2.2 and 1.4 to 1.5, respectively. The shapes of the excitation functions are consistent at 60° but not at 90°. To summarize, for $E_\gamma > 150$ MeV the Bates measurement is the only photodisintegration measurement in agreement with the capture results, and the Bonn and Saclay results are the only photodisintegration experiments which agree with each other.

The experiment reported here was performed with a large acceptance detector in a tagged photon beam. The large acceptance permits the simultaneous measurement of the complete angular distribution with minimal systematic error. The photon tagger reduces the uncertainty in determining the absolute photon flux normalization as well as providing a well-determined photon energy. This is the first reported measurement of ^{3}He(γ, pd) with a tagged photon beam.

II. EXPERIMENTAL SETUP

The experiment was performed using the tagged photon facility at the Saskatchewan Accelerator Laboratory [13]. The incident electron energy was 284 MeV with a typical duty factor of 40%. The primary collimator (20 mm in diameter) was located 194 cm from the radiator, which was 115 μm thick aluminum. The photon energy was determined by the photon tagging system with a resolution of ± 0.4 MeV, for a tagged photon energy range from 166 to 213 MeV. The overall uncertainty in the photon energy was approximately 4 MeV. The tagging efficiency was measured at frequent intervals throughout the experiment with a lead glass detector, which could be re-

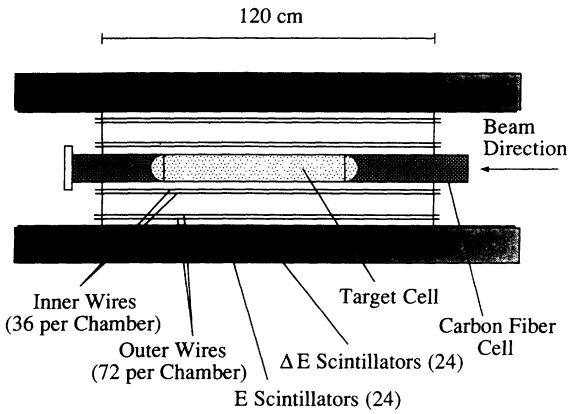

FIG. 1. Side view of SALAD.

motely moved into the beam path. These measurements necessitated lowering the tagger focal-plane rate from 1.2 MHz to about 400 Hz. The efficiency ($\epsilon_{\mathbf{tag}} = 0.756$), and thus the absolute photon flux, was determined to within 2.1%, averaged over the course of the experiment.

Charged particles produced by the tagged photon beam were detected in the Saskatchewan-Alberta Large Acceptance Detector (SALAD) [14]. The particle angle was determined by tracking through three cylindrical wire chambers (one of the four SALAD chambers was inoperative during this measurement). The particle energy was determined and the particle type was identified by 24 $\Delta E - E$ plastic scintillator segments surrounding the wire chambers. Figure 1 is a side view of the detector, which has cylindrical symmetry about the beam axis. A trigger threshold was applied to the sum of the ΔE and E signals from each segment to reduce electron triggers as described in Ref. [14]. The experiment trigger was formed from a coincidence between any two of the calorimeter segments and the tagger. The angular and energy resolution for this experiment are displayed in Figs. 2 and 3, respectively. The resolution along the length of the wires was measured with a collimated photon source and the results were input to a simulation of SALAD. The simulation was then used to generate Fig. 2. Figure 3 shows the energy resolution of the E scintillator, since this is typically the dominant contribution to the determination of the energy of the particle at its production vertex.

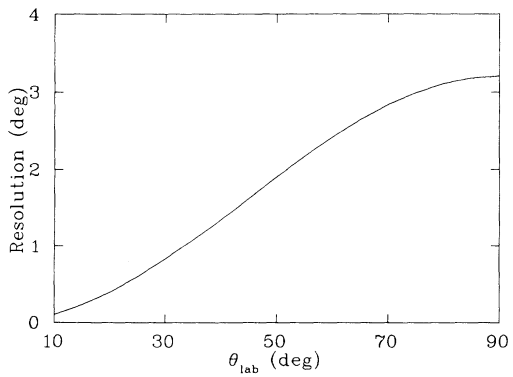

FIG. 2. rms angular resolution of SALAD as a function of laboratory scattering angle.

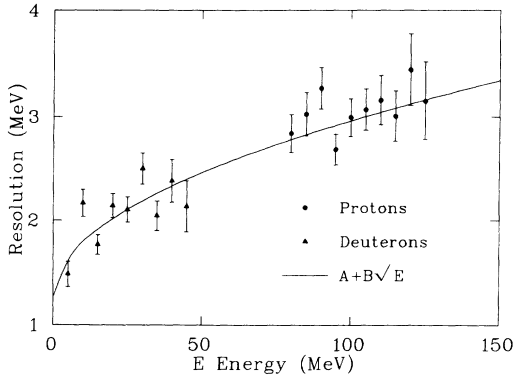

FIG. 3. rms energy resolution of SALAD for the E scintillator blocks. The solid circles and triangles are measured resolutions for protons and deuterons, respectively, from the ^{3}He(γ, pd) reaction. The solid line is a fit to the data of the form $A + B\sqrt{E}$.

The target was a cylinder of 0.036 cm aluminized Mylar containing ^{3}He gas at 255 kPa and room temperature. The 60 cm long cylinder was 10 cm in diameter. The instantaneous target temperature and pressure were monitored throughout the experiment to an accuracy $\leq$1%. The center of the cell was located 10 cm downstream of the center of SALAD. This corresponds to maximum geometric detection angles of 13°–169° in the laboratory frame. The angular coverage of SALAD, for single tracks, varied from 85 to 94 % of 4π along the length of the target cell.

The center of SALAD was located 451 cm downstream of the radiator. Since the average angle of photon emission is given by $m_e/E_e = 1.8$ mrad, this would imply a beam spot radius of 0.8 cm at the center of SALAD. The angle subtended by the primary collimator gives a radius of 2.3 cm at the center of SALAD, still well within the radius of the target.

III. DATA ANALYSIS

The acceptance of SALAD is determined via simulation. The large overdetermination of the kinematics for ^{3}He(γ, pd) allows for accurate verification of such items as total material thickness between the target and calorimeter, light output for protons and deuterons as a function of energy, attenuation lengths of the scintillators, and particle identification. The kinematics of the reaction were determined using the tagger measurement of the photon energy and the proton angle measured in SALAD. A χ^2 was then calculated from the other measured observables: energy deposition in the E and ΔE scintillators for the proton and deuteron, deuteron scattering angle, and coplanarity of the proton and deuteron. The particle type assigned to a track was determined by choosing the arrangement with the lower χ^2. The resultant reduced χ^2 distribution is displayed in Fig. 4, where the tracking cuts described below have been applied. The solid histogram is from a Monte Carlo simulation of the

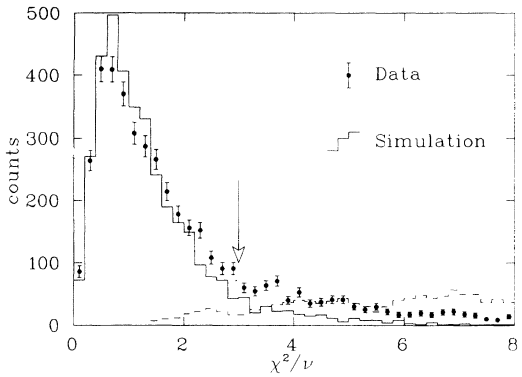

FIG. 4. χ^2 per degree of freedom for the ^{3}He(γ,pd) observables. The solid circles are the data with statistical errors and the solid histogram is a simulation of the detector. The arrow denotes the location of the cut applied. The dashed histogram is for simulated three-body breakup events.

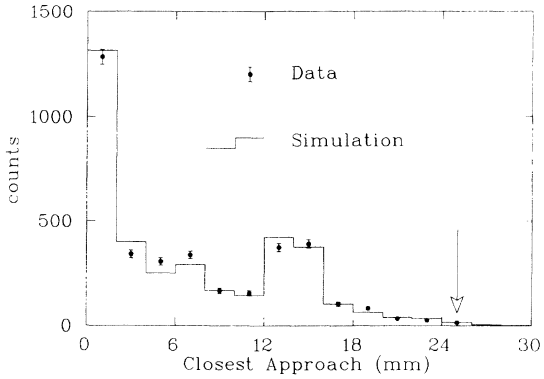

FIG. 6. Distance of closest approach of the tracks for the proton and the deuteron measured with SALAD. The solid circles are the data with statistical errors and the solid histogram is a simulation of the detector. The arrow denotes the location of the cut applied.

reaction and agrees with the measured distribution except in the tail region where the contribution from the three-body breakup of ^{3}He becomes significant. The arrow on the figure denotes the location of a cut applied to reject background events inconsistent with ^{3}He(γ, pd) kinematics. The contribution from ^{3}He(γ, pp)n remaining in the data set was estimated to be less than 5%. The χ^2 for simulated three-body breakup events, misidentified as two-body, is shown as the dashed histogram in Fig. 4.

Requiring that both tracks come from a point inside the target volume leads to cuts on the vertex location along the photon beam path, the perpendicular distance of the vertex from the photon beam path (Fig. 5), and the distance of closest approach of the two tracks to each other (Fig. 6). The bump near 14 mm in the closest approach distribution is a purely geometric effect stemming from the discrete ϕ values allowed by the wires in the tracking chambers. The solid histograms are from the simulation and the arrows denote the locations of the cuts applied. For Figs. 4–6 the statistics of the simulation were equal to that of the data.

Figure 7 shows the time difference between the tagger and SALAD after all cuts have been applied. This spectrum has been corrected for the photon flight path variation along the target length and for the propagation time in the scintillators. The peak is approximately 4.5 nsec FWHM with little background remaining from random coincidences. A window was placed about the peak at the indicated locations to reject random coincidence events. No subtraction of random events was done under the peak due to the low background observed. Random events remaining in the prompt peak are estimated to be less than 1%.

The detection efficiency as a function of proton center-of-momentum angle (θ_p^*) is displayed in Fig. 8 for the highest photon energy bin centered at 208 MeV (solid circles). This function was calculated from the simulation by taking the ratio of the number of Monte Carlo events which passed all analysis cuts relative to the total number of generated events. To reduce systematic uncertainties the same analysis software was used to analyze the Monte Carlo events and the experimental data. The error bars reflect the uncertainties in the thickness of

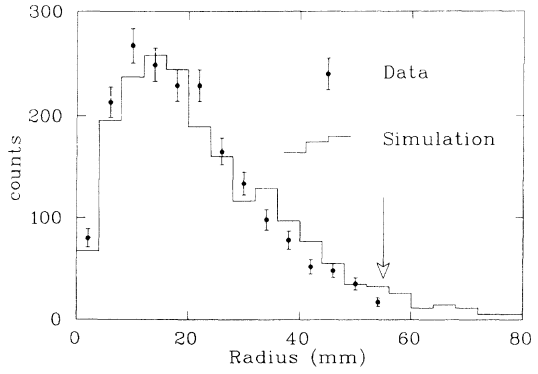

FIG. 5. Radius of the vertex as measured with SALAD. The solid circles are the data with statistical errors and the solid histogram is a simulation of the detector. The arrow denotes the location of the cut applied.

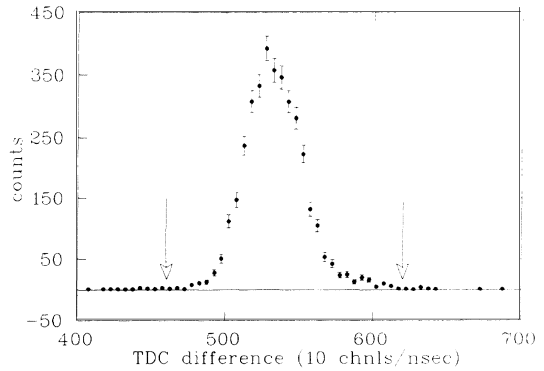

FIG. 7. Time difference in channels between the photon tagger and SALAD. The horizontal line denotes zero counts. The arrows denote the locations of the cuts applied.

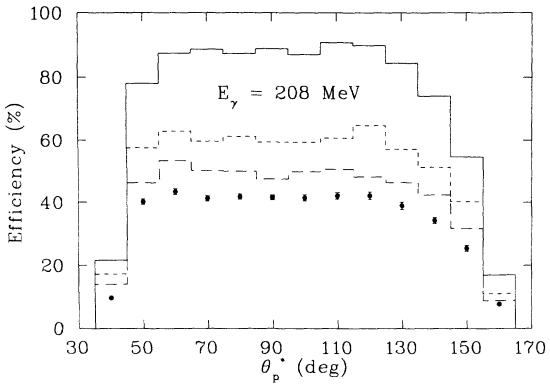

FIG. 8. Detection efficiency of SALAD as a function of proton center-of-mass system scattering angle, determined by Monte Carlo simulation, for a photon energy bin centered at 208 MeV (solid circles). The long-dashed histogram is a simulation without nuclear reaction losses in the calorimeter. The short-dashed histogram is without reaction losses and with 100% efficiency for the wire chambers of SALAD. The solid histogram is with only the applied the software cuts.

material between the target and the calorimeter, the nuclear reaction loss corrections for protons and deuterons in the scintillators, the effects of angular bin size, and the statistical uncertainty in the simulation. The reaction loss corrections were determined by GEANT for protons and found to be in good agreement with the compilation of Ref. [15]. For deuterons the calculations of Ref. [16] were used. The long-dashed histogram shows the simulated detection efficiency without nuclear reaction losses. The short-dashed histogram shows the detection efficiency without reaction losses and with the intrinsic efficiency of the wire chamber cells set to 100% in the simulation. The solid histogram shows the effect of only the software cuts on the detection efficiency. These cuts, described above, reduce the efficiency by 10%.

The normalization of the data was checked by measuring ^{2}H(γ,p)n with SALAD for photon energies from 180 to 220 MeV. This tests the photon flux normalization as well as the detection efficiency. The target for these measurements was a 2 m long gas cell [14] with 710 kPa of deuterium gas at room temperature. The results are displayed in Table I for a central photon energy of 200 MeV. The number in parentheses is the statistical error on the measurement. The quality of the current data do not permit extraction of cross sections at angles greater than 70° or less than 40° due to electron backgrounds in the detector. Further data taking is planned to improve these preliminary measurements. Also shown in Table I are recent results from LEGS for a photon energy of 200.8 MeV [17]. These have a systematic error of 5%. The agreement between the SALAD and LEGS results is within 10%. This is evidence that the overall normalization of the current experiment is understood within the quoted systematic uncertainty.

TABLE I. Center-of-mass system differential cross sections for ^{2}H(γ,p)n as a function of proton center-of-mass system scattering angle at a photon energy of 200 MeV. A systematic error of 5% for the LEGS data is not shown.

θ_p^* (deg)	$d\sigma/d\Omega^*$ (μb/sr)	
	SALAD	LEGS
40.748		4.492 (0.100)
45.0	4.11 (0.20)	
55.0	4.39 (0.20)	
64.710		5.048 (0.114)
65.0	4.50 (0.19)	
86.505		4.764 (0.110)

IV. DISCUSSION AND RESULTS

The final differential cross sections are shown in Fig. 9 and Table II for four photon energy bins spanning the tagger focal plane. The error bars include the statistical uncertainty in the data as well as angle-dependent errors on the calculated detection efficiency (Fig. 8). Other systematic errors on the cross sections not included in the errors in the figure and table are the uncertainty in the absolute tracking efficiency (9.5%), photon flux (2.1%), and target density (2%). If added in quadrature, these give an overall systematic error of 9.9% for the experiment. The relatively large systematic uncertainty in the tracking efficiency was due to one of the tracking cham-

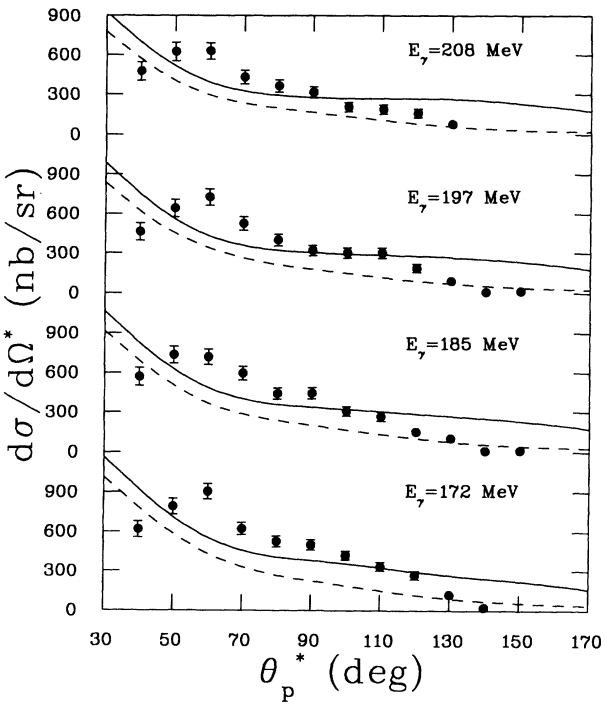

FIG. 9. Center-of-mass system differential cross sections for the two-body photodisintegration of ^{3}He as a function of proton center-of-mass system scattering angle, for four photon energy bins spanning the tagger focal plane. A systematic error of 9.9% is not included in the displayed error bars. The curves are calculations by Laget including two-body mechanisms (dashed) and a meson double-scattering diagram (solid).

bers being inoperative.

Figure 10 shows a comparison between different experiments for the highest photon energy bin of this experiment (E_γ = 203–213 MeV). The results of the other experiments have been adjusted to the central photon energy of 208 MeV, where appropriate, using the form $A(1/E_\gamma + B/E_\gamma^2)$. The adjustment factors A and B for a given experiment were determined from the results of that experiment. This correction did not exceed 3.3%. The agreement with the photodisintegration measurements at Bonn [10] and Saclay [9] is within the errors of the present experiment. The Bates [8] measurement is a factor of 1.3 higher which is just within the combined systematic and statistical errors of the two experiments. This factor of 1.3 holds true for all four photon energy bins measured in the present experiment. The capture measurements are higher by factors of 1.7 (4–5 standard deviations) for TRIUMF [6] and 1.2–1.8 (1.3–6 standard deviations) for SATURNE [7]. The shape of the TRIUMF angular distribution is consistent with the present experiment. The SATURNE data points at 95.6° and 105.0° (rightmost two open triangles in Fig. 10) were taken with an incident deuteron beam, in contrast to the point at 92.7° which was done with incident protons. The former angles are in agreement with the present measurement while the latter is in strong disagreement. This may indicate problems with the normalization of these capture data.

TABLE II. Center-of-mass system differential cross sections for ^{3}He(γ,pd) as a function of proton center-of-mass system scattering angle, for four photon energy bins. A systematic error of 9.9% is not included in the quoted errors shown in parentheses.

E_γ (MeV)	θ_p^* (deg)	$d\sigma/d\Omega^*$ (nb/sr)
208	40	475 (70)
	50	624 (70)
	60	629 (64)
	70	428 (52)
	80	363 (46)
	90	315 (43)
	100	206 (35)
	110	189 (34)
	120	160 (32)
	130	78 (25)
197	40	463 (65)
	50	642 (66)
	60	728 (64)
	70	524 (52)
	80	399 (45)
	90	320 (39)
	100	302 (39)
	110	300 (39)
	120	188 (32)
	130	90 (24)
	140	9 (9)
	150	15 (15)
185	40	570 (68)
	50	735 (64)
	60	719 (58)
	70	595 (51)
	80	443 (43)
	90	444 (43)
	100	308 (36)
	110	267 (34)
	120	151 (26)
	130	102 (24)
	140	8 (8)
	150	13 (13)
172	40	620 (61)
	50	792 (58)
	60	906 (57)
	70	624 (46)
	80	529 (42)
	90	503 (40)
	100	422 (37)
	110	333 (33)
	120	269 (31)
	130	121 (22)
	140	23 (11)

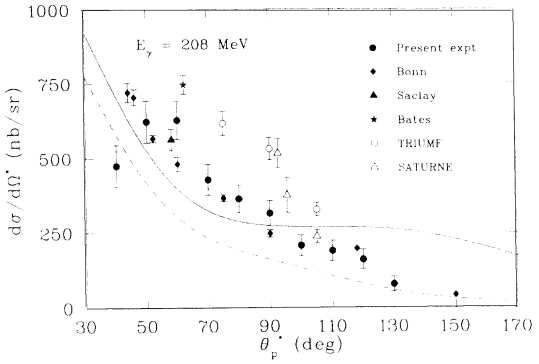

FIG. 10. Center-of-mass system differential cross section for the two-body photodisintegration of ^{3}He as a function of proton center-of-mass system scattering angle for a central photon energy of 208 MeV. The solid circles are from this experiment. Other results shown are from Bonn [10], Saclay [9], Bates [8], TRIUMF [6], and SATURNE [7]. A systematic error of 9.9% for the present experiment is not included in the displayed error bars. The curves are calculations by Laget including two-body mechanisms (dashed) and a meson double-scattering diagram (solid).

V. MODEL CALCULATIONS

Previous theoretical calculations have demonstrated the importance of meson-exchange currents in the two-body photodisintegration of ^{3}He, either through explicit diagrams [2, 18] or in a "quasideuteron" model [19, 20]. The latter calculations find good agreement with the proton capture and the Bates photodisintegration cross sections for a proton cms angle of 60°. The agreement is somewhat poorer at 90°. These two-nucleon model cal-

culations are presented in Refs. [6, 7]. No angular distributions are currently available from these calculations for the photon energies of the present experiment.

At photon energies of 240 and 340 MeV, the microscopic calculations of Laget [18] underpredict the differential cross sections for angles greater than about 60°. This discrepancy is significant as the two-body matrix elements are calibrated against ^{2}H(γ,p)n and the three-body wave function has been tested with ^{3}He($e,e'p$)^{2}H. Calculations by Laget [21] for the photon energies measured in this experiment are shown in Figs. 9 and 10. The dashed curves include all two-body absorption mechanisms. The solid curves include, in addition, a meson double-scattering mechanism which involves all three nucleons. In the central angular range, the calculation which includes meson double scattering is in better agreement with the data. However, the cross section is overpredicted at forward ($\theta_p^* < 50°$) and backward angles ($\theta_p^* > 120°$).

VI. SUMMARY AND CONCLUSIONS

We have measured the ^{3}He(γ,pd) absolute cross sections with tagged photons in four photon energy bins ranging from 166 to 213 MeV. The use of a large acceptance detector permitted coverage of the full angular distribution of the reaction while reducing systematic errors in the shape of the distribution. Our cross sections are consistently below the most recent photodisintegration experiment performed at Bates. The agreement with the TRIUMF and SATURNE proton capture measurements is poor, but the deuteron capture data from SATURNE are in agreement with the present experiment. We also find agreement, within the errors, with the older Saclay and Bonn photodisintegration measurements. The theoretical calculations of Laget are in reasonable agreement with the magnitude of our cross sections, but differ in shape, particularly at the extreme angles of this measurement.

[1] J. L. Friar, B. F. Gibson, and G. L. Payne, Annu. Rev. Nucl. Part. Sci. **34**, 403 (1984).

[2] J. M. Laget, *New Vistas in Electro-Nuclear Physics*, Vol. 142 of *NATO Advanced Study Institute, Series B: Physics*, edited by E. L. Tomusiak, H. S. Caplan, and E. T. Dressler (Plenum Press, New York, 1986), p. 361.

[3] N. M. O'Fallon, L. J. Koester, Jr., and J. H. Smith, Phys. Rev. C **5**, 1926 (1972).

[4] J. P. Didelez, H. Langevin-Joliot, Z. Marić, and V. Radojević, Nucl. Phys. **A143**, 602 (1970).

[5] M. A. Pickar, H. J. Karwowski, J. D. Brown, J. R. Hall, M. Hugi, R. E. Pollock, V. R. Cupps, M. Fatyga, and A. D. Bacher, Phys. Rev. C **35**, 37 (1987).

[6] J. M. Cameron *et al.*, Nucl. Phys. **A424**, 549 (1984).

[7] W. J. Briscoe, B. H. Silverman, D. H. Fitzgerald, B. M. K. Nefkens, A. Boudard, G. Bruge, L. Farvacque, and C. Glashausser, Phys. Rev. C **32**, 1956 (1985).

[8] D. I. Sober, H. Crannell, B. M. K. Nefkens, W. J. Briscoe, D. H. Fitzgerald, R. Goloskie, and W. W. Sapp, Jr., Phys. Rev. C **28**, 2234 (1983).

[9] P. E. Argan, G. Audit, N. De Botton, J.-L. Faure, J.-M. Laget, J. Martin, C. G. Schuhl, and G. Tamas, Nucl. Phys. **A237**, 447 (1975).

[10] H. J. Gassen, A. Hegerath, W. Loers, B. Mecking, G. Nöldeke, T. Reichelt, and H. Stanek, Z. Phys. A **303**, 35 (1981).

[11] P. Picozza, C. Schaerf, R. Scrimaglio, G. Goggi, A. Piazzoli, and D. Scannicchio, Nucl. Phys. **A157**, 190 (1970).

[12] C. A. Heusch, R. V. Kline, and K. T. McDonald, Phys. Rev. Lett. **37**, 409 (1976); C. A. Heusch, R. V. Kline, K. T. McDonald, and C. Y. Prescott, *ibid.* **37**, 405 (1976).

[13] J. M. Vogt, R. E. Pywell, D. M. Skopik, E. L. Hallin, J. C. Bergstrom, H. S. Caplan, K. I. Blomqvist, W. Del Bianco, and J. W. Jury, Nucl. Instrum. Methods Phys. Res. Sect. A **324**, 198 (1993).

[14] E. B. Cairns *et al.*, Nucl. Instrum. Methods Phys. Res. Sect. A **321**, 109 (1992).

[15] D. F. Measday and C. Richard-Serre, CERN Yellow Report CERN 69-17 (1969).

[16] D. F. Measday and R. J. Schneider, Nucl. Instrum. Methods **42**, 26 (1966).

[17] G. S. Blanpied *et al.*, Phys. Rev. Lett. **67**, 1206 (1991); private communication.

[18] J. M. Laget, Phys. Rev. C **38**, 2993 (1988).

[19] F. Prats, Phys. Lett. **88B**, 23 (1979).

[20] H. W. Fearing, in *Nuclear Physics with Stored, Cooled Beams (McCormick's Creek State Park, Spenser, Indiana)*, Proceedings of the Workshop on Nuclear Physics with Stored, Cooled Beams, edited by Peter Schwandt and Hans-Otto Meyer, AIP Conf. Proc. No. 128 (AIP, New York, 1984); Czech. J. Phys. **B36**, 263 (1986).

[21] J. M. Laget, private communication.

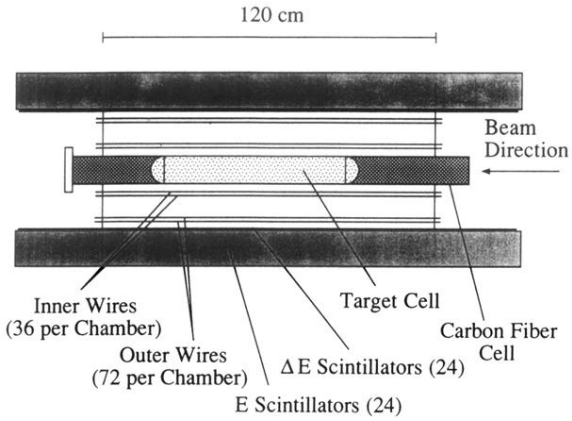

FIG. 1. Side view of SALAD.